PLIF Measurements of Nitric Oxide and Hydroxyl Radicals Distributions in Swirled Stratified Premixed Flames

J. Apeloig[1,*], P. Gautier[1], E. Salaün[1], B. Barviau[1], G. Godard[1], S. Hochgreb[2], F. Grisch[1]
1: CORIA - UMR6614, Normandie Université, CNRS, INSA et Université de Rouen, France
2: Dept. of Engineering, University of Cambridge, UK
* Correspondent author: julien.apeloig@coria.fr

Keywords: NO-PLIF, OH-PLIF, Swirled stratified premixed flames, Concentration, Flame thickness

ABSTRACT

Environmental and economic concerns have pushed aeronautical authorities to set stringent environmental regulations on fuel consumption, noise production, and pollutant emission. Engine manufacturers are developing novel staged injection concepts to ensure their respect. The injection staging creates a fuel-air mixture stratification involving new combustion processes not fully understood. This paper presents the experimental investigation of NO production for known swirled and/ or stratified lean premixed flames. The fuel staging parameter defined as the stratification ratio is studied for values of 1, 2, and 3, while the swirl fractions are 0, 25 and 33%, changing the flowfield from non-swirling conditions to high swirl numbers (up to 0.55). The implementation of simultaneous OH- and NO-PLIF imaging techniques is achieved using high energy pulsed laser systems, able, for instance, to deliver 30 mJ/ pulse around the 226-nm UV wavelength for NO excitation. OH-PLIF is used to characterize the flame structure through the commonly extracted curvature, and also through the measurement of the flame thickness. These results show to be more accurate than thickness obtained from temperature profiles measured by Raman/ Rayleigh laser diagnostics. NO-PLIF is used to quantify the pollutant concentration. To this end, preliminary work was done to select the $Q_1(29.5)$ transition as it the least temperature dependent excitation scheme with high fluorescence levels. After realizing a specific calibration of the NO-PLIF technique, the studied flames presented concentrations ranging from traces (20 ppm) to high levels (230 ppm). Further analysis of these results reveals that for high stratification ratios the prompt NO is favored and is responsible for the elevated level of NO pollutant.

1. Introduction

Increasing concerns about the effects of aeronautical engine emissions on the upper atmosphere, as well as at ground level around airports, have motivated stringent international environmental regulations (e.g. ACARE) to meet reduced aero-combustion emission levels. To that end, the aeronautical engine manufacturers have introduced new concepts of combustors that offer good potentialities to meet these severe restrictions. Designing such devices will be achieved using radially and/ or axially staged combustor architectures adding significant complexity that diminishes penalties for cost and weight onto the combustion system. One of the approaches concerns

the fuel staging that will integrate the pilot swirl stage within the lean premixing fuel swirl injector. These systems promote combustion in lean premixed-like regimes to control the flame temperature and consequently the pollutant emissions such as NOx and CO_2. For safety reasons, fuel and oxidizer are injected separately before entering the combustion chamber, therefore, in practice reactants are not perfectly mixed (non-uniform equivalence ratio) and stratified combustion regimes are observed. Mixture stratification is also present by design, to improve flame stability in overall lean combustion. In parallel to this physical mechanism, the interaction between turbulent coherent structures and inner combustion layer also plays a central role in premixed flames. Generally, these interactions are improved by producing swirling flow fields for a number of reasons. Swirling flows are known to assist flame stabilization by inducing or enhancing the recirculation of products into the flame. Greater levels of turbulence are also resulting from swirling flows, which can increase the heat release rate due to the growth of flame surface area. Mixing of fuel and oxidizer products can be enhanced but this effect can lead to unstable modes of operation. Such instabilities also promote the risk of upstream flame propagation toward the fuel injectors (flashback), which leads to the concerned components failure.

Despite widespread use, there is still an incomplete understanding of how swirl stratified premixed flame behave relative to premixed flames at a fundamental level. An extensive research was recently performed to study the effect of stratification on flame behavior for various operating conditions (laminar and turbulent) and burner geometry (v-shaped flame, bluff-body stabilized, piloted combustion bomb) (Anselmo-Filho et al., 2009), (Böhm et al., 2011) (Sweeney et al., 2011) (Vena et al. 2011). Providing a detailed probing of pollutant emissions inside of swirl stratified flames will complete our understanding of the effects of turbulence chemistry interaction processes on pollutant formation in such flames.

The objective of the present study was to investigate in detail the structure of swirl stratified methane-air flames using several laser diagnostics combined together. This effort is an extension of earlier experimental studies focused on the analysis of stratification and swirl effects on the flowfield characteristics of turbulent fuel-lean premixed flames (Sweeney et al., 2011) (Sweeney et al., 2012) (Zhou et al., 2013). A large panel of optical investigations has been done on this academic setup providing a good understanding of the aerodynamics and thermodynamics taking place in the various studied cases. To complete the data set and to enhance the entire understanding, a particular interest is given, among other things, to the role of the turbulent flame chemistry interactions on the NO reduction strategies.

In general, conventional gas sampling methods are used to measure the NO concentration but they are still limited when used for in-situ flame measurements because of their intrusiveness. On the contrary, laser light can be employed as an efficient non-intrusive measuring tool. The coherence of laser radiation permits a high spatial resolution whereas the availability of short pulses permits an extremely high temporal resolution enabling snap-shots of scalar parameters as species concentration, temperature, velocity and pressure (Boutier, 2013). With the purpose of measuring the concentration of NO in flames, the Planar Laser-Induced Fluorescence (PLIF) diagnostic has been selected. Until now, a large number of researches have been using PLIF diagnostics of gaseous fields at atmospheric pressure. Besides providing a sensitivity to trace quantities of radicals such as OH, it is also capable of resolving a wide range of spatial scales, and can provide temporal resolution to "freeze" the chemistry and fluid dynamics of reacting flows. For instance, many examples using OH-PLIF can be found in the literature (Grisch & Orain, 2009) (Kohse-Hoinghaus & Jeffries, 2002).

Regarding the detection of NO by LIF in flames, NO fluorescence measurements at atmospheric pressure and lean equivalence ratio present unique challenges not encountered when probing OH. The common strategy adopted by numerous researchers consists to perform single-point measurements in order to optimize the parameters affecting the fluorescence signals such as the dimensions of the probe volume and the intensity of the laser beam. Quantitative planar imaging of low NO levels is now undoubtedly more complex in flames since the laser intensity per pixel is usually less than with single-point measurements. From this point of view, the goal of this task was first to extend the capabilities of the NO-PLIF diagnostic to measure instantaneously the quantitative spatial distribution of NO when present in trace. The strategy adopted to optimize the fluorescence signals was first investigated through experiments performed in a high-temperature cell in which the behavior of the fluorescence signals were analyzed with temperature, collisional quenching and excitation wavelength. Then, the NO-PLIF diagnostic was combined with the OH-PLIF to simultaneously measure, into various swirl stratified flames, the NO production at its birth in relation with the flame structure.

2. Experimental procedure

An overview of the swirl stratified burner, operating conditions and experimental diagnostics is provided in this section.

2.1. Cambridge/Sandia Stratified swirl burner

The work presented in the current paper investigates the formation of NO pollutant from methane/ air premixed flames in a turbulent swirl burner initially designed by Cambridge University and Sandia National laboratories (Sweeney et al., 2012). This burner is a mockup of the actual prototypes developed by aeronautical engine manufacturers to generate reacting flow conditions representative of turbulent flows in practical systems, including sufficiently high turbulence levels, swirl, and operation under premixed and stratified combustion. The Cambridge/ Sandia burner (Fig. 1) consists of three concentric tubes in a laminar co-flow, but the center tube is sealed with a ceramic cap, and the flame is stabilized by recirculation of combustion products downstream of this central bluff body. Two independent fuel/ air injection circuits, the inner annulus and the outer annulus ones are used to inject premixed methane/ air flows at independent equivalence ratios offering the possibility to produce a stratification ratio to be varied. The outer annulus is also designed to perform experiments with or without swirling flows. To focus the analysis on the stratification and swirl ratio effects, the fuel circuits are designed to premixed methane/ air flows, and the sizing is developed to perform experiments at atmospheric pressure. The latest also simplifies the experimental set-up, removing the flame confinement that significantly reduces the complexity when using optical diagnostics.

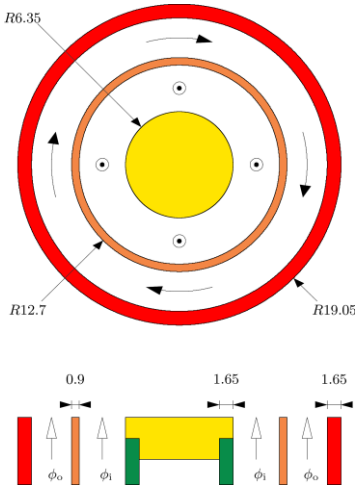

Fig. 1 Plan view of the exit geometry in the stratified swirl burner (SwB), showing a plan view and a cross section through the burner axis. The curved vectors in the plan view show the direction of swirling flows in the outer annulus, while the out of page vectors show the axial flow in the inner annulus. All dimensions are to scale and in mm. (Sweeney et al., 2012)

Case	*SFR*	ϕ_i	ϕ_o	*SR*
*SwB*1	0%	0.75	0.75	1
*SwB*2	25%			
*SwB*3	33%			
*SwB*5	0%	1	0.5	2
*SwB*6	25%			
*SwB*7	33%			
*SwB*9	0%	1.125	0.375	3
*SwB*10	25%			
*SwB*11	33%			

Table 1: Operating conditions (Sweeney et al., 2012)

The operating conditions for the present study are shown in Table 1. These conditions were selected to allow the investigation of flames in premixed and stratified regimes, with and without swirl. The stratification ratio, SR, defined as the ratio of the nominal equivalence ratio in the outer flow to that in the inner flow, was varied from 1 for lean premixed flames to 3 for the most stratified cases. The swirl fraction, SFR, denotes the percentage of outer flow rate through the swirl plenum to the total outer annulus flow. This value was varied from 0, for non-swirling flows, to 33%, for highly swirling cases, with a swirl number, SN~0.55 (Zhou et al., 2013).

2.2. PLIF configuration

The distribution of OH and NO was characterized using a combination of two PLIF systems. To that end, two pulsed laser systems are used to perform OH- and NO-PLIF measurements simultaneously (Fig. 2). Both systems are installed close to the test bench. Measurements of OH radicals are performed using a frequency-doubled, Q-switched Nd:YAG laser to pump a dye laser. The laser is frequency doubled to deliver wavelengths in the 280–290 nm spectral range, with an energy of 16 mJ per pulse. The dye laser is tuned to 282.75 nm to excite the $Q_1(5)$ line of the (1, 0) band of the OH ($X^2\Pi$–$A^2\Sigma^+$) system. Part of the laser beam is directed to the burnt gases of a reference laminar premixed methane–air flame in order to tune the laser to the aforementioned OH transition. The linewidth is estimated to be approximately 0.1 cm^{-1} by recording the spectral profile of several OH transitions in the reference flame. The $Q_1(5)$ transition is selected because of its high intensity, its well-isolated spectral feature and its low dependence upon temperature.

For NO excitation, the 532 nm beam from an injection seeded frequency doubled Nd:YAG laser was used to pump a Sirah PrecisionScan LG-2400 dye laser operating with a mixture of Rhodamine B and Rhodamine 590 dyes. The 615-nm output of dye laser was sum-frequency-mixed

with the third harmonic beam (355 nm) from the injection seeded Nd:YAG laser to produce 225.05 nm radiation required for one-photon laser-induced fluorescence. Generation of wavelengths around 226 nm by mixing is an alternative to the use of "classical" frequency doubled (SHG) blue dyes pumped by the frequency tripled YAG. The advantage of this approach is the superior lifetime of the dyes, the smaller spectral bandwidth of the generated UV radiation and the delivery of high energy/ pulse (up to 30 mJ/ pulse). Similarly as the OH-PLIF methodology, part of the laser beam is directed to the burnt gases of a reference laminar premixed CH_4/ air flame in order to tune the laser to the aforementioned NO transition. The linewidth is estimated to be approximately 0.7 cm^{-1} by recording the spectral profile of several NO transitions in the reference flame. As described in the next section, the $Q_1(29.5)$ transition has been selected to be excited in regards to its good fluorescence intensity that is barely linear with temperature variations.

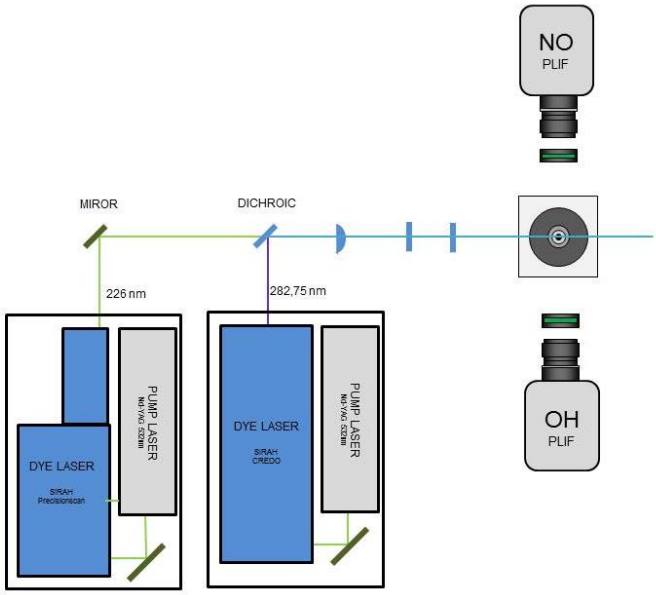

Fig. 2 Schematic of the experimental setup

Energy of both laser beams is controlled during the experiments by means of laser power meters. Time delay between the two laser beams is fixed to 100 ns in order to avoid cross-talks between fluorescence signals of OH and NO. This duration is much shorter than the typical flow timescale, ensuring that images of OH and NO fluorescence are representative of the same phenomenon at the time of recording.

Both laser beams are then transported via optical mirrors toward the burner and superimposed with a combination of dichroic mirrors. They are transformed into two superimposed collimated

sheets using a unique set of cylindrical and spherical lenses. The two cylindrical lenses form a telescope which spreads the beams into collimated sheets. Only the central zone of the laser sheets is used to obtain laser sheet energy profiles as flat as possible, allowing, in a first assumption, proportionality between the fluorescence signals and the probe species concentration. A spherical lens with 1-meter focal length is finally focusing the two sheets to a ~130 μm waist located in the center of the burner. Energy in the laser sheet is maintained to 4 mJ for OH and 6 mJ for NO detection, respectively. Fluorescence from OH radicals and NO are recorded with two 16-bit emICCD cameras (Fig. 3). Each camera used a CCD array of 1024 × 1024 pixels, a temporal gate of 70 ns, with a framing rate of 10 Hz and is equipped with a 105 mm, f/ 4.5 UV-NIKKOR lens. For OH measurements, the camera has a combination of a colored-glass filter (WG 295 from Schott) and an interferential filter centered at 315 nm (FWHM = 15 nm). For NO measurements, the camera is equipped with a 70-nm bandpass filter collecting NO fluorescence in the spectral range 230–300 nm. Each camera is interfaced to a personal computer used to control the camera and to record images. The gain of both ICCD cameras is adjusted to keep the energy recorded by the array detector proportional to the fluorescence signal issued from NO and OH, which prevents the emICCD cameras from local saturation. Laser pulses and camera gate triggering were synchronized using a delay generator.

Raw fluorescence images are corrected for black noise, background luminosity, non-uniformities in the collection optics and inhomogeneity in the laser sheet profile. An average background image is acquired with the laser on in air. The subtraction of this image from the fluorescence image corrects for laser scattering and other background luminosity. An average background image is also acquired with the laser off and the flame on in order to check that no flame emission was recorded in the same time.

3. NO Fluorescence strategy

The strategy taken to measure NO concentration in flames consisted first to select the most temperature-independent excitation transition for NO excitation. To this end, the temperature dependence of NO-LIF signal was studied using a high-temperature cell. Fluorescence of NO is obtained using excitation of various rotational lines in the $A^2\Sigma^+ \leftarrow X^2\Pi$ (1, 0) transition near 226 nm. This band has been well characterized spectroscopically and is well convenient experimentally for fluorescence measurements in flame environments (Battles & Hanson, 1995). The probe volume beam energy is limited to less than 10 μJ to ensure that fluorescence is within the linear excitation regime. As an example of results, the resulting NO-LIF emission spectra are shown in

Fig. 3. The spectra are recorded in a NO/ N_2 mixture (0.1% NO) at atmospheric pressure after excitation of the $Q_1(18.5)$ transition for various temperatures ranging from 300 to 880 K. As observed on this figure, the intensity of the emitted fluorescence is not varying linearly with the temperature. Repeating the record of the fluorescence spectra for other excitation wavelengths and integrating each of the fluorescence spectra over the bandwidth of the optical filters used with the PLIF imaging technique, the excitation of the $Q_1(29.5)$ transition was selected in regards to its good fluorescence intensity that is barely linear with temperature variations.

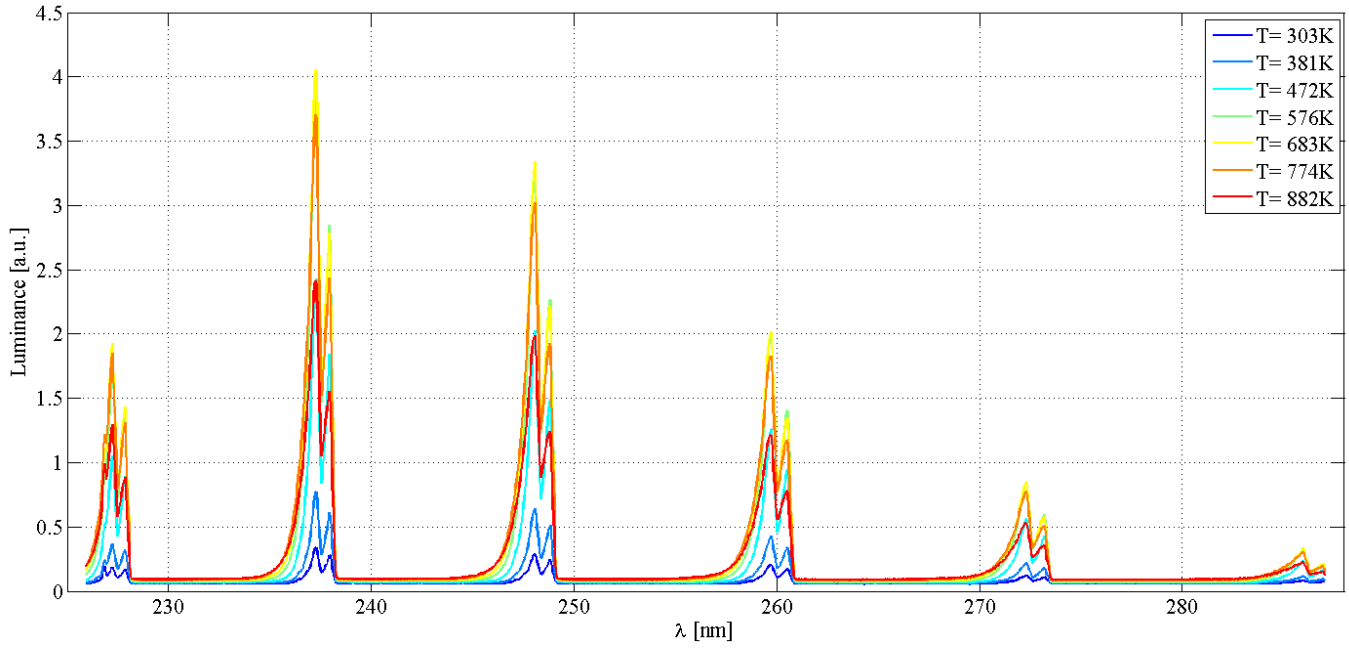

Fig. 3 Evolution of the NO $A^2\Sigma^+ \leftarrow X^2\Pi$ (1, 0) fluorescence emission spectra from excitation of the $Q_1(18.5)$ transition (λ=225.72 nm) with respect to temperature. Pressure = 0.1 MPa.

Another complication which has been evaluated for the quantification of the NO fluorescence is the effect of the interaction of the NO fluorescence with the fluorescence of molecular oxygen in the Schumann-Runge B←X system. This system, described extensively by Krupenie (1972), is the strongest electronic transition in O_2 and has features which extend from below 200 nm to near 300 nm. Although many of these features are weak in terms of absorption line strength, they can cause substantial interference in the lean flames pertinent to this work, where the O_2 concentration in the product gas region may exceed ppm-levels. To evaluate this potential limitation, the NO fluorescence spectrum was recorded in a laminar premixed CH_4/ air flame formed with a reference porous burner. The used equivalence ratio was 0.7 yielding a mole fraction of 6% for O_2 and a level of 10 ppm for NO. From the analysis of the excitation fluorescence spectrum, it has been confirmed that the $Q_1(29.5)$ line does not interfere with the fluorescence of the neighboring

O_2 transitions, validating then its choice to perform quantitative measurements of NO concentration in lean flames.

Finally, as the measurement of the local NO concentration relies upon the proportionality between the fluorescence intensity and the NO concentration, the observed signal intensity S_{LIF} can be written as:

$$S_{LIF} \propto N(T)F^{LIF}(T,\gamma_{coll}(T)) \quad (1)$$

where the function F^{LIF} indicates the effect of the spontaneous-emission rates and collision-energy transfer processes. For our study, the total quenching rate has been estimated for lean-flame conditions using the data of Paul et al. (1994) and the composition of gas and temperature distributions taken from previous studies on the same burner (Sweeney et al., 2012) (Kamal et al., 2015).

Since the LIF signals were temperature-dependent, the absolute number density of NO was calibrated in flames in which species concentrations, temperature, and pressure were well-known. The calibration of the NO signal was performed in a laminar, premixed flame of CH_4 + air stabilized upon a sintered bronze plate (Grisch et al, 1996). The evolution of the fluorescence signal has been measured with NO concentration at low equivalence ratio. For that, the flame was doped with various amounts of NO. This calibration assumed that most of the doped NO passed through the flame zone without participating in the reburn-reactions and that the amount of natural NO is small compared to the doped amount. The former assumption is supported by the experimental studies of (Schulz et al., 1999), who suggest that measurements of [NO] by LIF must be calibrated under fuel-lean conditions and with NO-dopant levels of > 200 ppm. Furthermore, the calculations performed using the CHEMKIN and PREMIX codes (Kee et al., 1985) (Kee et al., 1989) indicated that [NO] in the burnt gases is within 2% of the doped level. Based on this, the relative accuracy of the measurements of [NO] was estimated to be about 5 % (Grisch et al, 1996).

4. Results

This section presents simultaneous PLIF measurements of OH radical and NO pollutant at the outlet of the stratified burner for different operating conditions. In the first part, spatial correlation between OH and NO fluorescence is discussed. The second part of the section presents the

influence of combustion parameters (stratification ratio, swirl) on OH and NO spatial distributions.

4.1. Correlation between OH and NO fluorescence

Long-exposure photographs of the flame at various conditions are shown in Fig. 4 (left). The first (upper) one corresponds to a non-swirling flame with a stratification ratio of 3. The second (middle) one shows the case of a swirling flame (SRF=25%) with a stratification ratio of 2. The last (lower) one is the case of a combustion with the highest swirling ratio (SRF=33%) and no stratification (SR=1). As observed on these photographs, the expansion variation of the flame is clearly evident when comparing the three operating conditions. In the same time, the flames are all attached and stabilized on the central bluff body. These results are corroborated when examining the OH-PLIF images displayed in Fig. 4 (center). These images show the spatial and instantaneous distribution of OH fluorescence corrected from the laser sheet inhomogeneity. All the OH images are scaled with the same color bar. These images are recorded downstream from the bluff body on a region of 80 mm x 50 mm. The laser sheet travels from right to left in the images.

As mentioned previously, OH-PLIF acts as a marker of the regions with high temperature namely, the reaction zone and the hot burned gases. For non-swirling flames, the highest OH LIF signals are attributed to super-equilibrium OH concentrations that are formed in the reaction zone. OH is therefore conveyed towards the center of the flame under the action of the inner recirculation. Presence of uniform high-level of concentration of OH (typically, a factor of 3-5 lower than the peak concentration levels) along the center of the flame is also observed. Although there is no reaction zone in this region, local OH radicals in this region subsists because of the high-level of temperature (Sweeney et al., 2012). Taking into account these considerations, it appears that the reaction zones are governed by a steep increase in OH concentrations and they can accordingly be identified by the large gradients of the OH-PLIF distributions. The inner recirculation zone also contributes to the flame stabilization as the shear layer attaches the flame to the bluff-body. Finally, the analysis of the OH-PLIF distributions show that the flame is mainly propagating without expansion while the flame edges present large scale undulations and corrugations.

Increasing the swirling ratio modifies the flame expansion as observed in Fig. 4. The flame is progressively opening due to the incoming of unburned fresh gases inside the core of the flame. This effect is well demonstrated on the results recorded for SFR=33% in which a significant reduction of OH fluorescence signals in the core of the flame is noted. Furthermore, gradient of

OH concentration appears to dominate parts of the central flowfield due to the mixing between OH and incoming fresh gases. Furthermore, an increase of the wrinkling of the flame front is highlighted with a formation of cusps and unburned mixture fingers. At maximum SFR, the flame front topology is highly distorted with significant changes in the structure, both spatially and temporally.

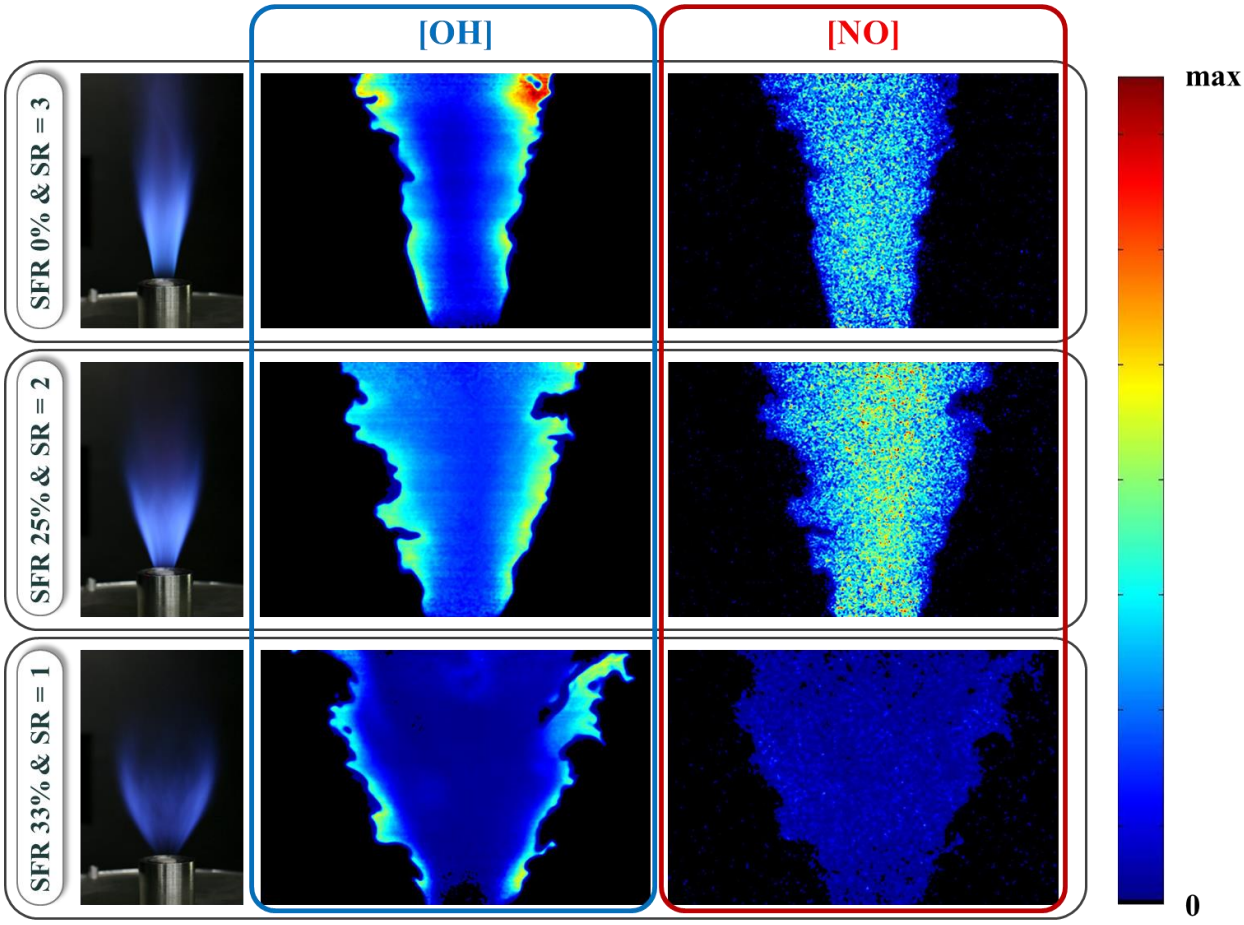

Fig. 4 Left: long-exposure photographs of the flames studied in the current work. Center: instantaneous distributions of OH. Right: instantaneous distributions of NO.

The resulting instantaneous images of NO concentration distributions are also displayed in Fig.4 (right) for the same operating conditions. All the images use the same concentration color-scale 0-250 ppm according to the calibration procedure described previously. A conjoint analysis of both OH and NO distributions reveal that the signals never overlap. The turbulent structures observed at the frontier of the NO region and at the contours of the OH distribution (i.e. the flame front) are constantly adjacent. This was supported by the combination of a thin reaction zone with a fast reaction mechanism. For these operating conditions, the NO distribution is quite

homogeneous in space and in time, indicating that NO when formed in the reaction zones are transported towards parts of the core of the flow under the action of the inner recirculation zone. Furthermore, the large production of OH into the reaction zone (i.e. governed by the presence of steep gradient of temperature) indicates that the major part of NO is preferentially produced by thermal NOx formation which is highly temperature dependent.

A conjoint analysis of PLIF measurements performed for the nine operating conditions investigated in the current work give new insights regarding the combined effect of stratification and swirl on production/ reduction of NO pollutant. For instance, for non-swirling flows, the increase of stratification from 1 to 2 leads to a significant boost of NO concentration, passing from 70 to 160 ppm. Beyond this value, a stabilization of NO production is then observed. Same trends are also observed with swirling flows excepting when SFR=33%. In the latest case, NO concentration increases from 20 ppm to 230 ppm when SR is moving from 1 to 3. Now regarding the effect of the swirling fraction, a decrease of NO is noted for SR=1 when increasing the swirling fraction while an opposite trend is recorded for SR= 3. This results in an increase of NO of about 50 % when SFR varies from 0 to 33%. Contrary to a "classical" premixed swirling flame in which NO is preferentially spawn from NOx thermal process (i.e. governed by temperature), the existence of similar levels of temperature in these given flame conditions (Sweeney et al., 2012) cannot explain this increase of NO concentration. When a high level of stratification is chosen, an increase of the swirl intensity is locally changing the equivalence ratio gradients across the instantaneous flame front then enhancing the efficiency of the prompt NO process whilst maintaining an elevated level of temperature.

4.2. Flame structure analysis from OH-PLIF

As observed in Fig. 4, the hydroxyl radical, OH, is the chemical product the most spawned during the swirl stratified premixed CH_4/ air under study. The observation of the existence of OH quantity growing quickly within the reaction zone makes this radical growth rate a sensitive maker of the flame front. These information can be commonly used to isolate the unburnt and the burnt gases (Dumont et al., 1993), hence, allowing the analysis of the flame contour, which gives information about the flame curvature and therefore its surface density function (Lee et al., 2000). The post-treatment developed during this study intends to use this characteristic to measure the flame thickness and to visualize the flame reaction rate.

4.2.1. Flame contours and curvature

The post-treatment procedure to extract the flame front geometry operated on the OH-PLIF images is similar to the procedure described and applied by Sweeney et al. (2011 and 2012), on these study cases. First, the 16-bit OH-PLIF images are converted to binary images using a threshold technique. The threshold used varies from case to case as the OH radical production changes for each condition. The threshold is also adapted for the near-border region as the intensity decreases as a border effect, even after correcting for the laser intensity distribution. For this operation, the OH-PLIF images are split into two half flames, i.e. left and right. This procedure facilitates the discrimination of the burnt and unburnt gases during the scanning phase. The flame front geometry is then revealed by the contour of the resulting binary image. The 2-D Cartesian profile is converted to curvilinear coordinates. Local curvature is then obtained by performing a moving analysis along the profile, fitting a third-order polynomial over 15 points, and computing its value using Eq. 2 (Bayley et al., 2012). The post-treatment procedure to obtain the local curvature of the flame front is exemplified in Fig. 5.

$$\kappa_d = \frac{\frac{dy}{ds}\frac{d^2x}{ds^2} - \frac{dx}{ds}\frac{d^2y}{ds^2}}{\left[\left(\frac{dx}{ds}\right)^2 + \left(\frac{dy}{ds}\right)^2\right]^{\frac{3}{2}}} \qquad (2)$$

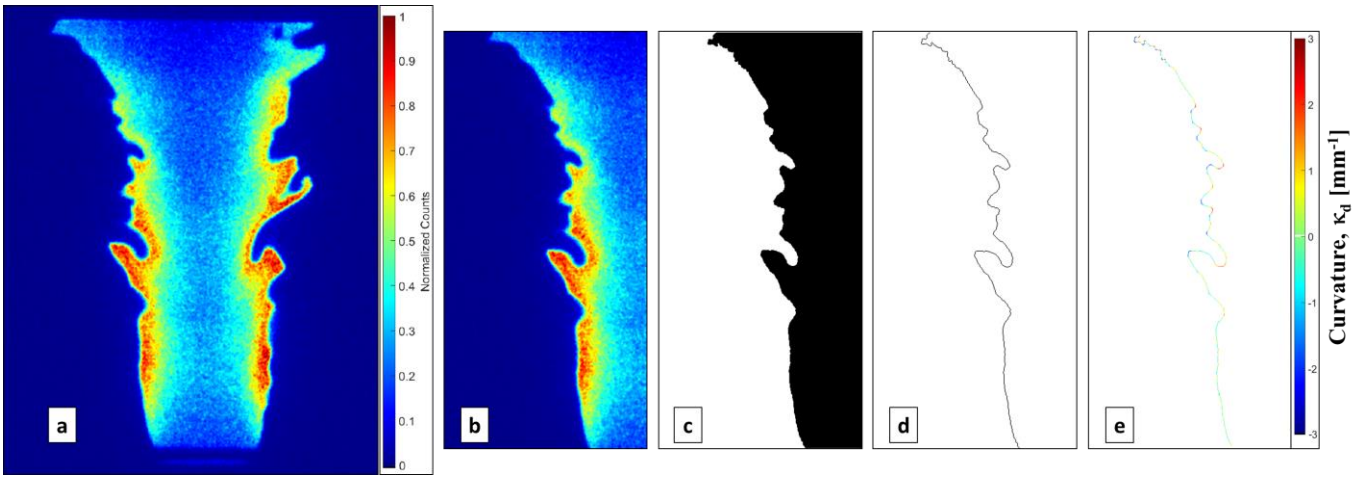

Fig. 5 Sample of OH-PLIF post-treatment to obtain the local curvature. a: uncorrected raw OH-PLIF. b: left half of the OH-PLIF to be processed. c: binary image of the OH-PLIF revealing unburnt gases in white and burnt gases in black. d: contour of the flame geometry. e: local curvature.

The comparison of the probability density functions (PDF) of the local flame front curvatures obtained on experiments and measurements performed at University of Cambridge and at CORIA Laboratory is in good agreement (Fig. 6). These results prove a good repeatability of the experiments, and confirm the distribution of the local curvature. This analysis of the flame front geometry was also performed for the swirled study cases, and similar observations are made.

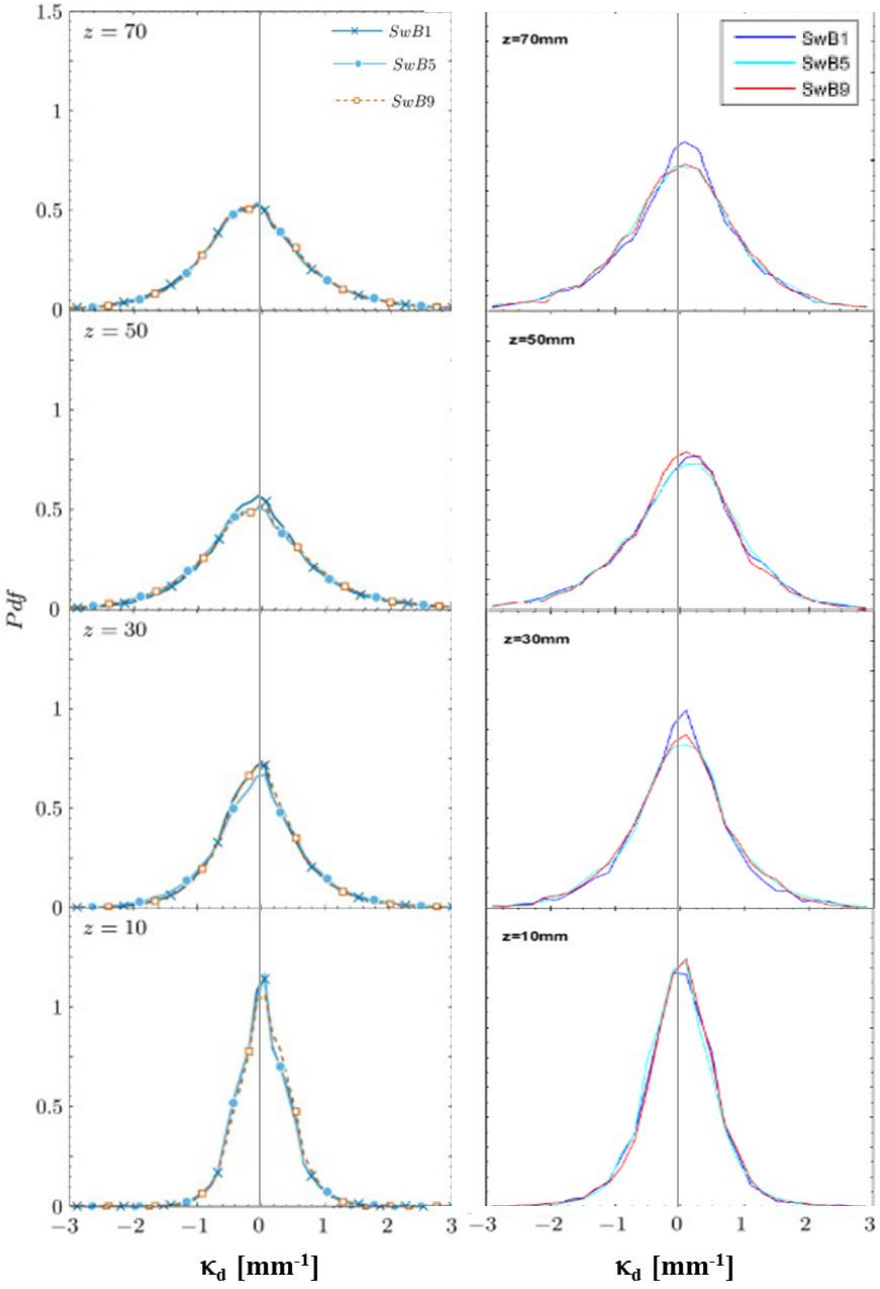

Fig. 6 Probability density functions of the flame curvature for various locations away from the injection plane (z = 10, 30, 50, and 70 mm - bottom to top), and the three non-swirling study cases (SwB1, SwB5, and SwB9), from experiments performed at University of Cambridge (left - adapted from Sweeney et al., 2011) and at CORIA (right).

4.2.2. Flame thickness and reaction rate distribution

The post-treatment procedure starts from the corrected OH-PLIF images (Fig. 7-a). These corrections account for the dark noise, and the laser energy distribution. Hence, the Prewitt operator is applied to obtain the magnitude of the 2-D gradient (Fig. 7-b), corresponding to the growth rate of the OH radical. The following step uses the threshold technique to convert the OH growth rate image into a binary image. The threshold value is chosen to keep only the quickly growing points. In this work, the threshold was set to 1/ 5^{th} of the maximum OH count. Isolated points or small groups are removed to obtain Fig. 7-c. A hysteresis routine is then run to eliminate the small ligaments in contact with the flame front Fig. 7-d. This routine scans the neighboring area of each point, and keeps the ones validating conditions of minimal length and width of connecting points. These minima are defined from preliminary analysis of the various study cases, and results of previous studies (Sweeney 2012). Knowing that the flame thickness varies between 0.4 - 1.6 mm, and that a 69-µm/ pixel spatial resolution was obtained with the optical setup, the minimum length is set to 6 connecting pixels and to 3 for the width. This technique limits the recovery of flame fronts thicker than 3 pixels, or 207 µm. Improvements to routine could allow the conservation of thinner flame fronts to the detriment of the uncertainty. If one wants to observe thinner flame fronts, the optical arrangement must be modified to obtain a better spatial resolution. Using magnifiers, a 10-µm/ pixel spatial resolution can obtained.

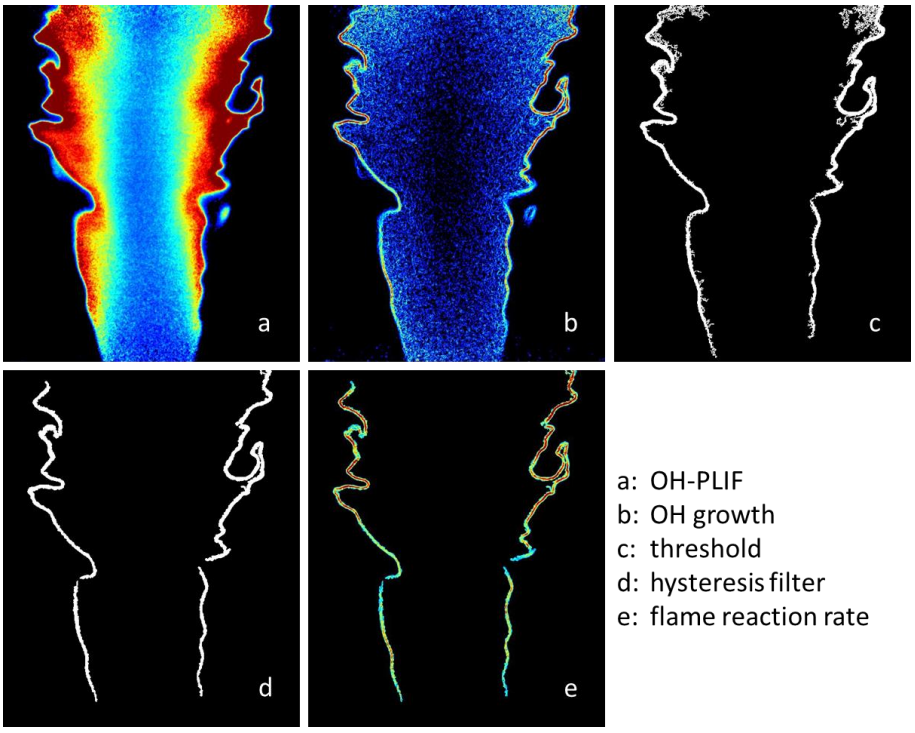

Fig. 7 OH-PLIF image post-treatments extracting the flame thickness and the flame reaction rate distribution.

Finally, the flame thickness is directly analyzed from this binary image by integrating the data along the radial location for various distances from the injection plane. It is also interesting to use this binary image (Fig. 7-d) as a mask applied on the OH growth rate (Fig. 7-b), to reveal a qualitative image of the flame reaction rate (Fig. 7-e).

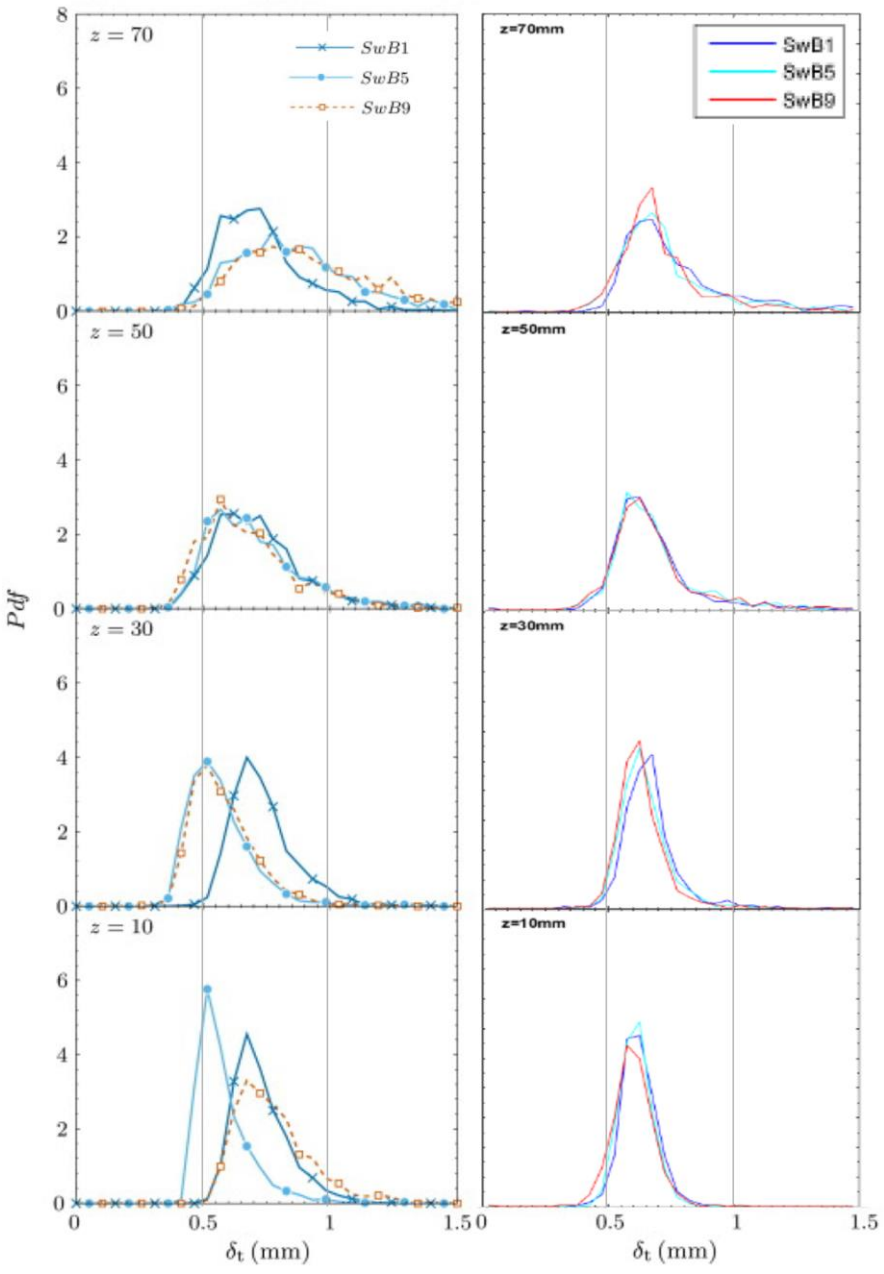

Fig. 8 Probability density functions of the flame thickness for various locations away from the injection plane (z = 10, 30, 50, and 70 mm - bottom to top), and the three non-swirling study cases (SwB1, SwB5, and SwB9), from experiments performed at University of Cambridge (left - adapted from Sweeney et al., 2011) and at CORIA (right).

In a similar manner as the comparison of flame local curvatures, the flame thickness probability density functions obtained by University of Cambridge and by CORIA Laboratory are compared. For this comparison, it is important to notice that the thicknesses reported by Sweeney et al. (2011 and 2012) are computed from temperature measurements, whereas the results reported in this paper are calculated from the OH radical growth parameter. The comparison in Fig. 8 presents solely the results for the non-swirled cases. This comparison shows similar shapes of PDFs for the study cases, and the same growth of the flame thickness as distance from the injection plane increases. However, the results obtained from the OH-PLIF image processing reveals better coherence between the three cases for z= 10 and 30 mm than the results obtain by Sweeney et al. (2011).

This preliminary result shows high potential for further investigation and analysis of flame/ pollutant interaction. This future work will focus on correlating the flame characteristics such as its curvature, flame thickness, reaction rate and temperature to the NO local formation.

5. Conclusions

Experimental investigations concerning major aspects of swirled stratified lean premixed combustion, including reaction progress and NO pollutant formation have been performed. The potential of laser diagnostic techniques was demonstrated. Observations from swirled stratified premixed methane/ air flames operated with different stratification ratios and swirl fractions were reported. The laser techniques include planar laser-induced fluorescence (PLIF) of OH simultaneously with PLIF of NO. In particular, NO-PLIF diagnostic has been developed to measure instantaneously the distribution of NO concentration into the investigated flames operating at atmospheric pressure. This diagnostic offers the potential to instantaneously map the spatial distribution of NO concentration with a signal-to-noise ratio allowing the fractional detectivity of few ppm of NO, present in such flames. This diagnostic was applied on the Cambridge/ Sandia burner to complete the large database of results on swirled stratified lean premixed flames already available, therefore improving the understanding of the physical processes governing the NO formation. The main conclusions regarding stratification are as follows:
In a general manner, stratification elevates the NO levels disregarding the swirl ratio investigated. Furthermore, the effect of the swirl fraction for a given stratification ratio induces different trends. At moderate levels of stratification, the NO levels are attenuated in function of the swirl intensity while an increase of NO in function of the swirl intensity is observed for high level of stratification. This last effect could be consequent to higher rates of the prompt NO mechanism

compared to the thermal NOx process, when the equivalence ratio tends to be rich (case of high level of stratification). In this last situation, as the inner equivalence ratio is rich, the prominence of the prompt NO mechanism to the thermal NOx could explain the increase of the NO levels.

In addition, the simultaneous OH-PLIF images recorded allow a confrontation of the flame characteristics (curvature, thickness, reaction rate) to the NO formation and distribution. The novel post-treatment technique presented allows extracting the size of the flame thickness from the OH-PLIF images. Further investigation of the results pulled out from this technique combined with the NO-PLIF analysis will improve the understanding and will gives better insights on pollutant formation.

All these results have some implications for the applicability of premixed flames in real combustors. The promising technique of simultaneous OH- and NO-PLIF is to be further developed in order to be applied in high-pressure combustors. The first step will be to extend the experimental validation to high-pressure and high-temperature levels. Afterwards, the end-goal will be to implement this laser diagnostic to quantify the NO formation in new ultra-low NOx injection systems operating at nominal conditions.

References

Anselmo-Filho P, Hochgreb S, Barlow RS, Cant RS (2009) Experimental measurements of geometric properties of turbulent stratified flames. Proc Combust Inst. doi:10.1016/ j.proci.2008.05.085

Battles B, Hanson RK (1995) Laser-induced fluorescence measurements of NO and OH mole fraction in fuel-lean, high-pressure (1–10 atm) methane flames: Fluorescence modeling and experimental validation. J Quant Spectrosc Radiat Transfer. doi:10.1016/ 0022-4073(95)00020-L

Bayley A, Hardalupas Y, Taylor A (2012) Local curvature measurements of a lean, partially premixed swirl-stabilised flame. Exp. Fluids. doi: 10.1007/ s00348-011-1181-4

Böhm B, Frank JH, Dreizler A (2011) Temperature and mixing field measurements in stratified lean premixed turbulent flames. Proc Combust Inst. doi:10.1016/ j.proci.2010.06.139

Boutier A (2013) Laser Metrology in Fluid Mechanics. John Wiley & Sons, Hoboken, NJ USA. doi:10.1002/ 9781118576847

Dumont JP, Durox D, Borghi R (1993) Experimental Study of the Mean Reaction Rates in a Turbulent Premixed Flame. Combust Sci Tech. doi: 10.1080/ 00102209308924110

Grisch F, Attal-Tretout B, Bouchardy P, Katta VR, Roquemore WM (1996) A vortex-flame interaction study using four-wave mixing techniques. J Nonlinear Optic Phys Mat. doi:10.1142/ S0218863596000349

Grisch F, Orain M (2009) Role of Planar Laser-Induced Fluorescence in combustion research. Aerospace Lab 1.

Kamal M, Barlow RS, Hochgreb S (2015) Conditional analysis of turbulent premixed and stratified flames on local equivalence ratio and progress of reaction. Combust Flame. doi:10.1016/ J.combustflame.2015.07.026

Kee RJ, Grear JF, Smooke MD, Miller JA (1985) A Fortran Program for Modeling Steady Laminar One-Dimensional Premixed Flames. Sandia National Lab Rep SAND85-8240.

Kee RJ, Rupley FM, Miller JA (1989) CHEMKIN II: A Fortran chemical kinetics package for the analysis of gas-phase chemical kinetics. Sandia National Lab Rep SAND89-8009.

Kohse-Hoinghaus K, Jeffries J (2002) Applied Combustion Diagnostics. Combustion: An international series, Taylor & Francis, London, UK.

Kuprenie PH (1972) The Spectrum of Molecular Oxygen. J Chem Phys Ref Data. doi:10.1063/ 1.3253101

Lee SY, Seo S, Broda J, Pal S, Santoro R (2000) An Experimental Estimation of Mean Reaction Rate and Flame Structure During Combustion Instability in a Lean Premixed Gas Turbine Combustor. Proc Combust Inst. doi: 10.1016/ S0082-0784(00)80280-5

Paul PH, Gray JA, Durant J.W, Thoman JW (1994) Collisional quenching corrections for laser-induced fluorescence measurements of NO A2Sigma(+). AIAA J. doi:10.2514/ 3.12158

Schulz C, Sick V, Meier UE, Heinze J, Stricker W (1999) Quantification of NO A–X (0, 2) laser-induced fluorescence: investigation of calibration and collisional influences in high-pressure flames. Applied Optics. doi: 10.1364/ AO.38.001434

Sweeney MS, Hochgreb S, Barlow RS (2011) The structure of premixed and stratified low turbulence flames. Combust Flame. doi:10.1016/ j.combustflame.2011.02.007

Sweeney MS, Hochgreb S, Dun MJ, Barlow RS (2012) The structure of turbulent stratified and premixed methane/ air flames II: Swirling flows. Combust Flame. doi:10.1016/ j.combustflame.2012.05.014

Vena PC, Deschamps B, Smallwood GJ, Johnson MR (2011) Equivalence ratio gradient effects on flame front topology in a stratified iso-octane/ air turbulent V-flame. Proc Combust Inst. doi:10.1016/ j.proci.2010.06.041

Zhou R, Balusamy S, Sweeney MS, Barlow RS, Hochgreb S (2013) Flow field measurements of a series of turbulent premixed and stratified methane/ air flames. Combust Flame. doi:10.1016/ j.combustflame.2013.04.007